(Received 7 November 2024, Accepted 12 December 2024, Scheduled 25 December 2024)

A Frog-Shaped UWB MIMO Antenna Design for 5G

Shanhua Yao[1], Tianchu Yang[1,*], Xiaorong Qiu[1], and Xiang Li[2]

[1] School of Electrical and Information Engineering, Anhui University of Science and Technology, Huainan 232001, China
[2] School of Computer Science, Huainan Normal University, Huainan 232001, China

ABSTRACT: In this paper, a frog-shaped ultra-wideband (UWB) multiple-input multiple-output (MIMO) antenna is proposed for 5G applications in the n77, n78, n79, and 6 GHz bands with a compact antenna structure of $31 \times 55 \times 1.5\,\text{mm}^3$. The designed antenna consists of two frog-shaped monopole antennas and a floor from which a part has been removed, and the operating bandwidths range from 3.05 to 13.38 GHz, which meets the design criteria for UWB. The T-shaped floor with two T-shaped slots impedes the flow of coupling currents and improves the isolation of the antenna. This results in an isolation of less than −17 dB over the entire operating bandwidth and less than −20 dB in the 5G band. In addition, the envelope correlation coefficient (ECC) is less than 0.007, the diversity gain (DG) more than 9.96, the total active reflection coefficient (TARC) less than −30 dB, and the channel capacity loss (CCL) less than 0.34 bit/s/Hz. The measured and simulated results agree with each other, demonstrating the antenna's potential application in 5G communication systems.

1. INTRODUCTION

5G communication is a widely used communication method nowadays, and antenna is an important part of contemporary communication networks. Therefore, the design of 5G antennas has attracted extensive research, and due to the limitations of millimeter waves and the expensive cost of millimeter wave devices, researchers have focused on 5G midwave band antennas. Most 5G systems operate in the frequency bands n77 (3.3–4.2 GHz), n78 (3.3–3.8 GHz), n79 (4.4–5 GHz), and 6 GHz band (6.4–7.1 GHz) was classified for 5G by the Ministry of Industry and Information Technology (MIIT) in 2023 [1], which is a brand-new frequency band used for 5G communications. The continuous development of communication technology promotes the continuous expansion of radio spectrum, UWB technology impedance bandwidth, high transmission data rate, and multipath cancellation, which promotes the UWB antenna technology to be used in 5G cellular communication. The band range of UWB antennas has been designated as 3.1–10.6 GHz by the Federal Communications Commission (FCC) [2]. MIMO antenna systems associated with UWB technology provide a linear increase in capacity with respect to the number of antennas, allowing for a significant increase in antenna transmission efficiency without the need to add additional spectrum or increase power resources. However, antenna design is affected by mutual coupling and spatial correlation between antenna elements [3, 4].

In recent years, planar antennas for 5G wireless communications and UWB MIMO have been extensively studied. In [5–10], antennas were desinged by special shaped patches. Ref. [5] used a circular patch to determine the 3.5 GHz resonance point and an inverted L-shaped slot floor for decoupling and isolation. However, the antenna has a large size of 44 mm × 46 mm. In Addepalli and Anitha's work in 2021, a compact MIMO antenna is described that uses parasitic reflectors and a protruding ground structure to isolate the antenna below −20 dB [6]. In [7], a metamaterial structure is used for isolation, and an antenna bandwidth of 2–18 GHz is obtained, but the isolation is just below −15 dB. Ref. [8] describes a high bandwidth circular MIMO antenna. The antenna uses rectangular parasitic cells and inverted L-shaped rectangular patches to provide isolation below −20 dB over the entire operating bandwidth (3–20 GHz). As presented by Siyara et al., a two-port MIMO antenna based on a metamaterial array is described using a low-profile substrate with a compact ring-split ring resonator cell metamaterial structure, allowing the antenna to have a frequency range of 1–15 GHz with an isolation of −20 dB or less. However, the antenna has a relatively large size of 26.5 mm × 112 mm [9]. In [10], a novel chair-shaped compact MIMO antenna is presented, which exhibits an operational bandwidth of 3–6 GHz.

In [10–14], the trenching technique is employed to enhance the isolation of MIMO antennas. The antenna in [10] employs triangular slots and parasitic cells to enhance the isolation between the two ports. Nevertheless, the isolation of the antenna is less than −13 dB. In Kumar et al.'s work in 2023, two pairs of inverted L-shaped open patches are employed for the purpose of port isolation, resulting in an antenna isolation of as low as −52 dB [11]. As presented by Chakraborty et al., a 4-port elliptical internal MIMO antenna with rectangular slots is presented as a means of enhancing the isolation between its constituent elements. However, the isolation of the antenna is below −14 dB and has a large size of 80.5 mm × 127 mm [12]. In [13], isolation is reduced by a stepped EBG structure and T-shaped floor with an inverted H-shaped slot, which are driven inversely to each other, thus reducing the isolation, and demonstrates the feasibility of the method by eigenmode analysis. As detailed

* Corresponding author: Tianchu Yang (2023200724@aust.edu.cn).

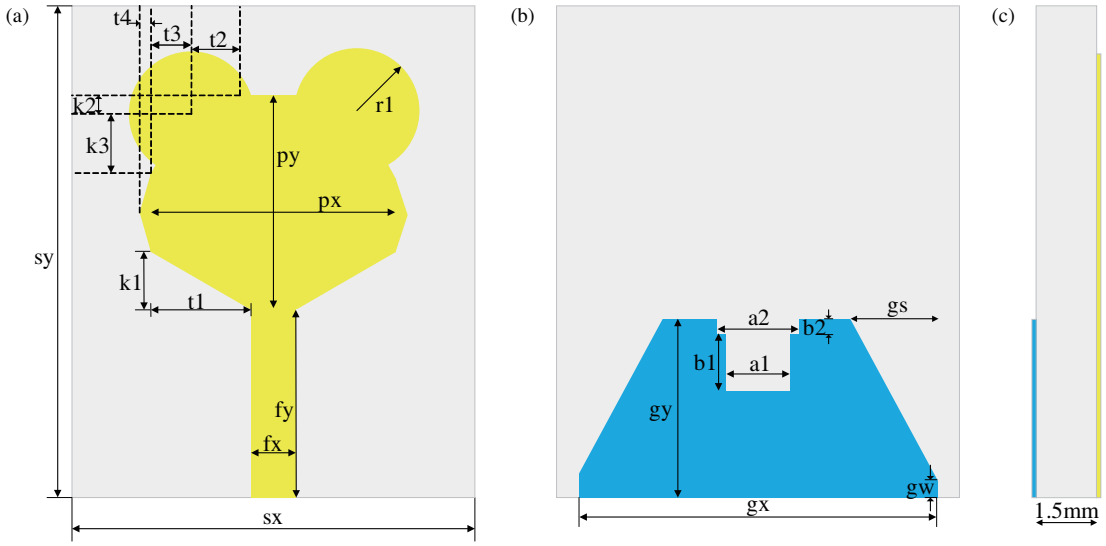

FIGURE 1. Single-element antenna structure: (a) top view, (b) bottom view, (c) side view.

in [14], a wideband dual-element millimeter-wave MIMO antenna has been developed which employs a modified T-shaped decoupling structure to achieve a reduction in isolation to below −20 dB.

In [15–18], the isolation of the MIMO antenna is enhanced by modifying the positional relationship between the antenna units. The single-element antenna introduced in [15] consists of a large torus internally tangent to six intersecting smaller cirques, and the MIMO antenna is in the form of a + shape, with the single-element antenna orthogonal to the quad ends. However, this antenna has a relatively large size of 90 mm × 90 mm. As presented by Abdelghany et al., a 4-port neighboring octagonal MIMO antenna is described. The antenna employs four orthogonally positioned individual elements to enhance the isolation between ports, resulting in a minimum isolation of less than −20 dB between ports. However, the antenna has a relatively large size of 60.5 mm × 62.5 mm [16]. In [17], a two-port MIMO antenna is presented, comprising two single-element antennas positioned orthogonally and a T-shaped floor inclined at 45° serving as an isolation structure, thereby achieving an isolation level below −21.5 dB. Kansal et al.'s work in 2024 provides a detailed description of a self-isolating 5G antenna with the high isolation of −22 dB or less. However, the bandwidth of the antenna is only 2.5–4.5 GHz [18]. Nevertheless, the above literature has some limitations, such as the antenna has a large size; the bandwidth is not wide enough; the resonance point is not in a specific frequency band; and the isolation and decoupling performance is not optimal.

In accordance with the aforementioned scheme, this paper presents a novel antenna structure and design methodology for 5G applications in the n77, n78, n79, and 6 GHz bands. The proposed compact frog-shaped UWB MIMO antenna features an enhanced isolation between ports, achieved through the utilization of a T-shaped ground structure with T-slots. The designed antenna operates in the frequency range of 3.05–13.38 GHz, and the resonance points are within the n77, n78, n79, and 6 GHz bands. The antenna exhibits favorable gain, directivity, ECC, and CCL characteristics in specialized broadband applications, including those pertaining to 5G technology.

2. SINGLE-ELEMENT ANTENNA DESIGN

2.1. Antenna Structure

In this paper, a compact frog-shaped UWB monopole antenna for 5G applications in n77, n78, n79, and 6 GHz bands is proposed. The antenna is fabricated on a substrate with dimensions of 25 mm × 31 mm and thickness of 1.5 mm, which consists of standard FR4 material with dielectric constant (ε_r) of 4.4 and loss tangent ($\tan\delta$) of 0.02. The substrate of this material is lossy, which is related to the thickness of the substrate. The antenna proposed in this paper has a thickness of 1.5 mm with low profile which reduces the losses to some extent. Figure 1 depicts the configuration of the designed frog shaped UWB antenna. The structural dimensions of the designed antenna are shown in Table 1.

2.2. Stages of Antenna Design Evolution

As shown in Figure 2, the design evolution of the antenna is divided into four steps. In the first step, a rectangular microstrip antenna as shown in Figure 2(a) is derived from Equations (1)–(4). c is the speed of light in air, f the frequency, L the resonant length of the patch, w its width, h the thickness of the substrate, and ε_r the effective dielectric constant of its dielectric. As can be seen in Figure 3, a narrower frequency band is provided by the antenna. In the second step, the rectangle on the front side of the antenna is cropped, and the floor is narrowed to obtain the antenna as in Figure 2(b), which widens the bandwidth of the antenna considerably. In the third step, two rectangles are dug in the center of the floor to obtain the antenna as in Figure 2(c), so that the antenna gets two resonance points. In the fourth step, two circular patches are obtained from Equations (5) and (6) as the eyes of the frog, and an isosceles triangle is

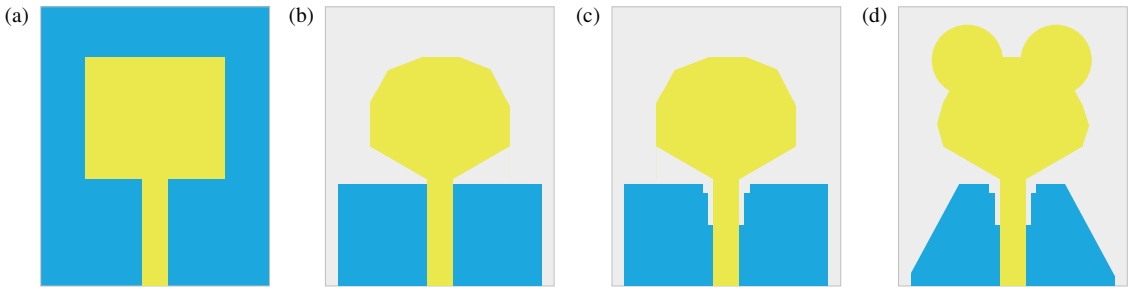

FIGURE 2. Design flow of single-element antenna: (a) Ant1, (b) Ant 2, (c) Ant 3, (d) Ant 4.

TABLE 1. Dimensions of single-element antenna structures.

Parameters	sx	sy	gx	gy	gs	gw	fx	fy	px	py	k1
Value (mm)	25	31	24	9.5	6.6	1	3.2	10.9	17	15.4	3.1
Parameters	k2	k3	t1	t2	t3	t4	a1	a2	b1	b2	r1
Value (mm)	3.4	4.1	6.9	4	1.28	0.55	4	4.8	3.2	0.9	4.9

TABLE 2. Dimensions of the MIMO antenna structure.

Parameters	W	L	W1	W2	W3	W4	W5	W6
Value (mm)	55	31	26	6	1	6.25	2.65	1.5
Parameters	W7	L1	L2	L3	L4	L5	L6	R2
Value (mm)	3	1	2	14.9	0.5	0.6	3.9	2.5

added on each side as the face of the frog to obtain the antenna as shown in Figure 2(d). F_{rc} is the circular undercut of the resonant frequency in GHz. Finally, two right-angle triangles are dug out on both sides of the floor to complete the design of the frog-shaped UWB antenna.

$$L = \frac{c}{2f\sqrt{\varepsilon_{eff}}} - 2\Delta L \tag{1}$$

$$\Delta L = 0.412h\frac{(\varepsilon_{eff}+0.3)\left(\frac{w}{h}+0.262\right)}{(\varepsilon_{eff}-0.258)\left(\frac{w}{h}+0.813\right)} \tag{2}$$

$$\varepsilon_{eff} = \frac{\varepsilon_r+1}{2} + \frac{\varepsilon_r-1}{2}\left(1+\frac{12h}{w}\right)^{-\frac{1}{2}} \tag{3}$$

$$w = \frac{\lambda_0}{2}\left(\frac{\varepsilon_r}{2}\right)^{-\frac{1}{2}} \tag{4}$$

$$R = T\left[1+\frac{2h}{\pi T\varepsilon_r}\left(\ln\left(\frac{\pi T}{2h}\right)+1.7726\right)\right]^{-\frac{1}{2}} \tag{5}$$

$$T = \frac{8.719\times10^9}{\sqrt{\varepsilon_r}F_{rc}} \tag{6}$$

From Figure 3, the operating bandwidth of the frog-shaped UWB antenna is 2.93–12.94 GHz, and the resonance points are 3.4 GHz, 6 GHz, 8.7 GHz, and 11.5 GHz, respectively.

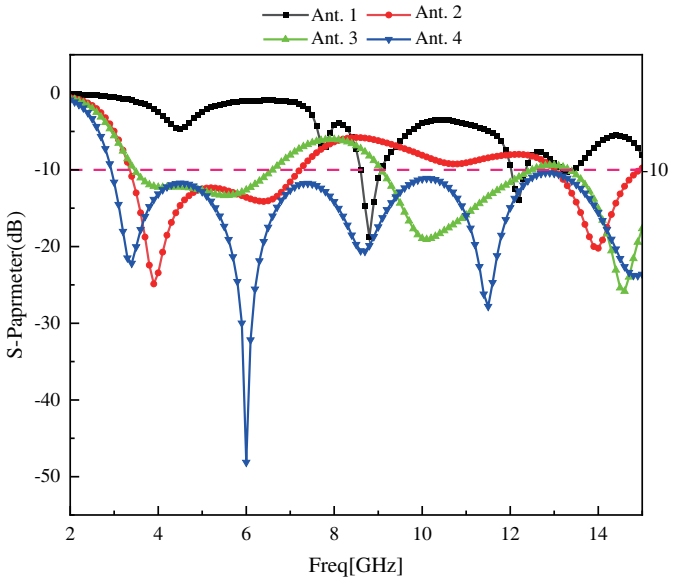

FIGURE 3. Simulation results of four antennas.

2.3. Antenna Parameter Analysis

The width gs of the cut triangle and the height gy of the floor have a significant impact on the performance of the antenna. To optimize these parameters, HFSS software is employed to achieve the optimal performance of the antenna. As illustrated in Figure 4, the bandwidth of the antenna initially increases and then declines with rising gs, reaching its peak at a value of gs equal to 6.6 mm. Similarly, Figure 5 depicts that the bandwidth of the antenna initially rises and then declines with increasing gy, reaching its maximum at a value of gy equal to 9.5 mm.

3. MIMO ANTENNA DESIGN

3.1. Antenna Structure

Figure 6 shows the geometry of the two-ended frog-shaped UWB MIMO antenna. The antenna is fabricated on a substrate

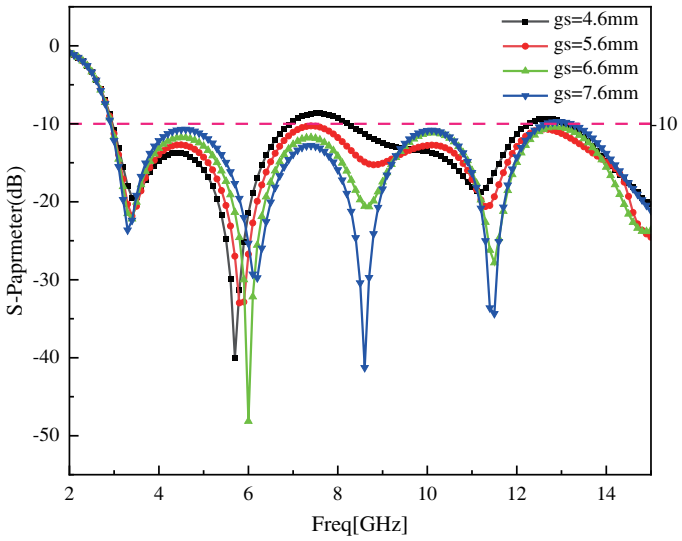

FIGURE 4. Effect of gs parameter on antennas S_{11}.

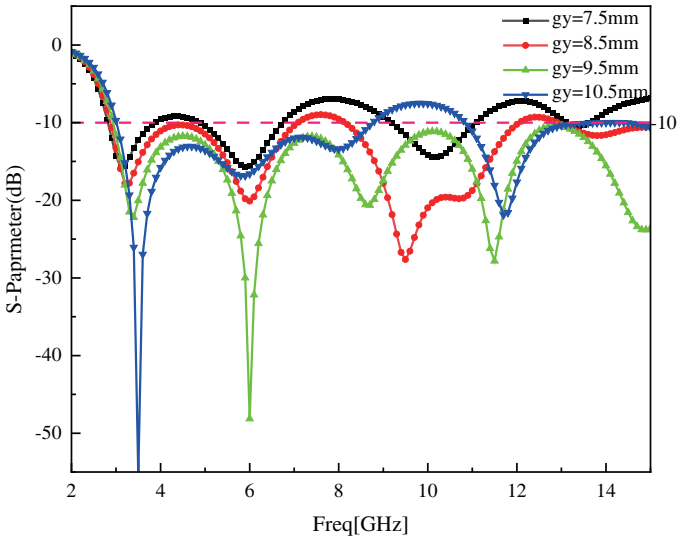

FIGURE 5. Effect of gy parameter on antennas S_{11}.

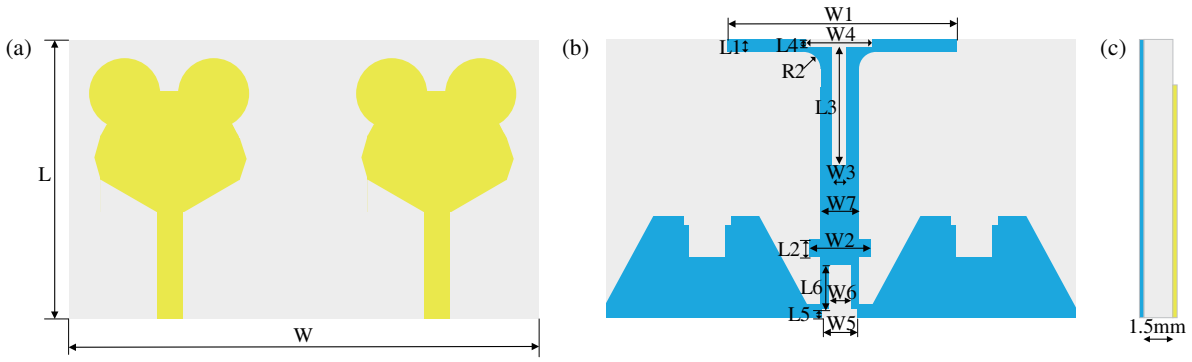

FIGURE 6. UWB MIMO antenna structure: (a) top view, (b) bottom view, (c) side view.

with dimensions of 55 mm × 31 mm and a thickness of 1.5 mm, which consists of standard FR-4 material. The antenna consists of two symmetrically positioned radiating patches on the substrate, whose feeding mechanism is realized through a microstrip line configuration. To have a high degree of isolation between the antenna ports, the intersection of the T-shaped stub was made circular, and then the T-shaped stub was attached to the floor. A T-slot and an inverted T-slot were dug at the top and the bottom of the T-shaped stub, respectively, and a rectangular patch was added in the middle of the two T-slots. The structural dimensions of the designed antenna are shown in Table 2.

3.2. Stages of Antenna Design Evolution

The shape of the floor is continuously improved to enable the design of the UWB MIMO antenna with good bandwidth and decoupling. The design evolution of the antenna is shown in Figure 7 in four steps. In the first step, a single-element antenna is placed symmetrically on both sides of the substrate, and the floors of both are connected by a rectangular strip. Since decoupling structure is not used, the S_{11} parameters are not much different from the single element at this point, but the isolation reaches up to −10.6 dB, so it still needs to be further reduced. In the second step, the use of a T-shaped plate promotes improved decoupling between neighboring antennas. At this point, the isolation will be below −18 dB, but the operating bandwidth of the antenna changes to 5.1–15.4 GHz, which is not in the ideal operating bandwidth. In the third step, the intersection of the T-floor is rounded, and a rectangular patch is added underneath it to add a new resonance point at 6.6 GHz. In the fourth step, a T-slot and an inverted T-slot are dug at the top and bottom of the T-shaped floor, respectively. So the bandwidth of the antenna is enlarged, and the isolation is less than −17 dB overall.

The final antenna operating bandwidth is 3.05–13.38 GHz as shown in Figure 8(a), and the resonance points are 3.5 GHz, 4.7 GHz, 5.9 GHz, 6.6 GHz, 9.1 GHz, 10.6 GHz, and 11.9 GHz. As shown in Figure 8(b), the isolation of the operating bands is less than −20 dB except for 8.7–10.2 GHz.

3.3. Antenna Parameter Analysis

The size of the T-slot dug in the floor and the rectangular patch added have a significant effect on the performance of the antenna, and parameters $L3$ and $W7$ were optimized using HFSS

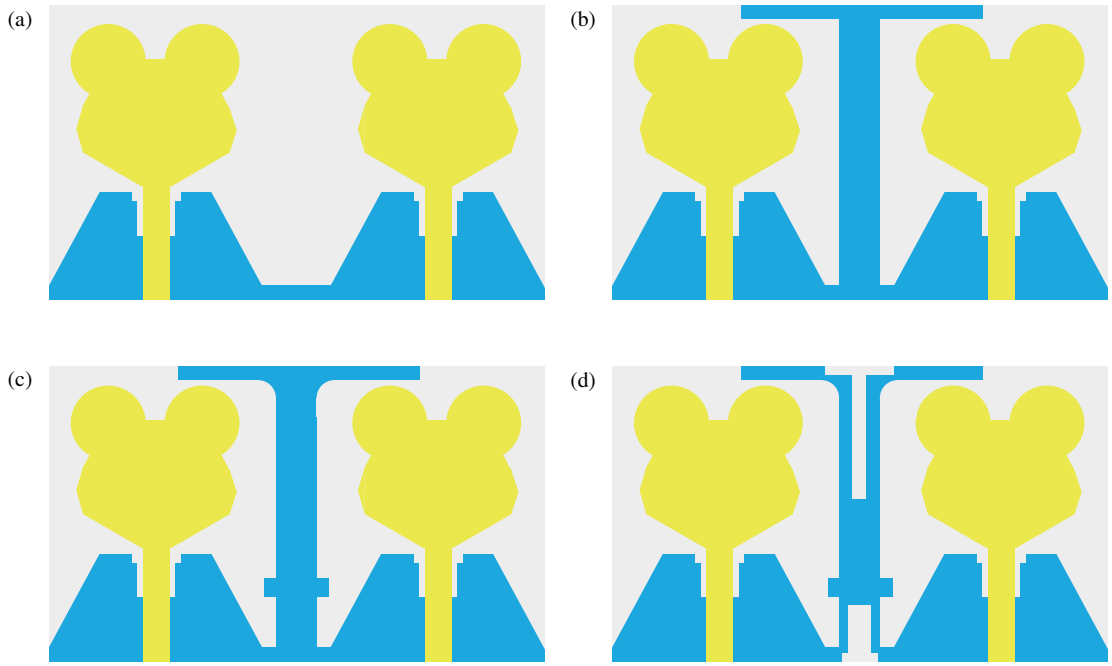

FIGURE 7. Design flow of UWB MIMO antenna: (a) Ant 1, (b) Ant 2, (c) Ant 3, (d) Ant 4.

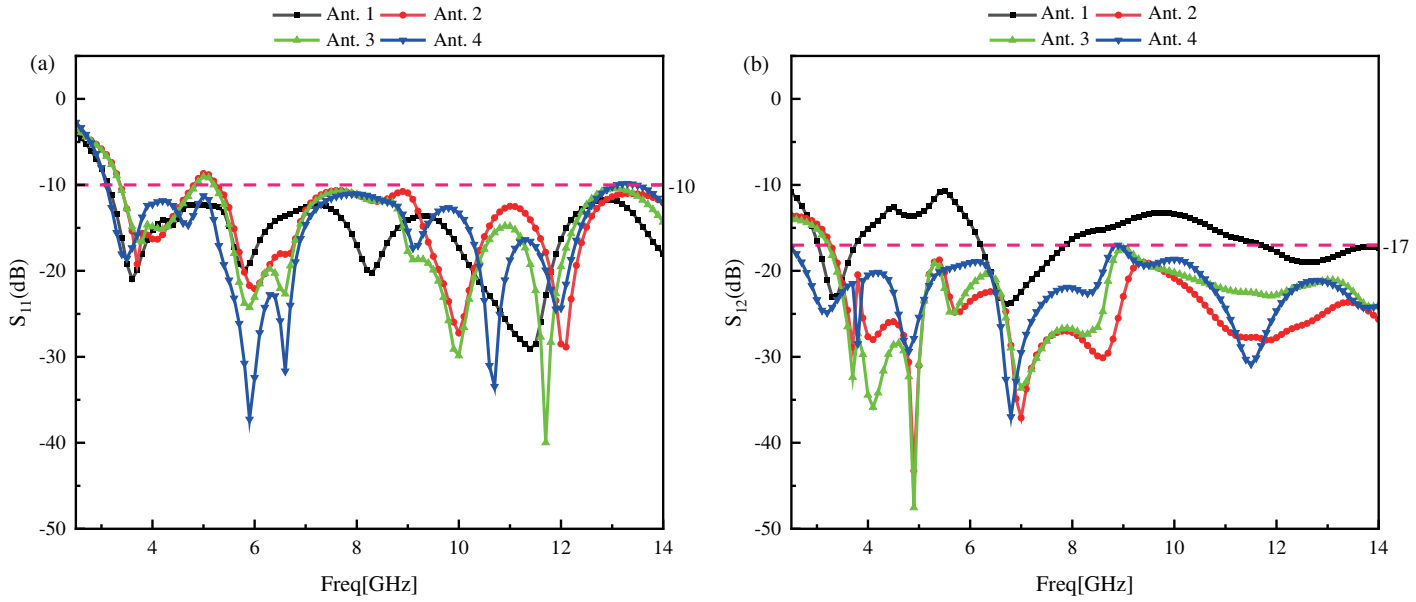

FIGURE 8. Simulation results of four antennas: (a) S_{11}, (b) S_{12}.

software to achieve the best performance of the antenna. The antenna bandwidth increases with the increase of $L3$ as shown in Figure 9(a). The value of $L3$ also affects the isolation between the ports as shown in Figure 9(b). When the value of $L3$ is 15.4 mm, the antenna has a better operating bandwidth and isolation decoupling effect with an ideal resonance point. As shown in Figure 10(a) for 5–6 GHz, S_{11} rises with the increase of $W7$ and is greater than -10 dB at a value of $W7$ of 5 mm. As shown in Figure 10(b), $W7$ has a significant effect on the isolation between ports. The antenna has good operating bandwidth and isolation when the value of $W7$ is 3 mm.

3.4. Antenna Current Analysis

Figure 11 shows the surface current distribution of the four antennas, aiming to enhance the decoupling effect of MIMO antennas by analyzing the surface currents of the MIMO antennas. As shown in Figure 11(a), a new defective floor is formed by a rectangular patch that connects the floors of two single-element antennas and is excited at port 1. Simulations using HFSS software show that a large amount of current is coupled to port 2. In Figure 11(b), a T-shaped floor is used, and only a small amount of current is coupled to port 2. In Figure 11(c), the intersection of the T-shaped floor is rounded, and a rectangular patch is

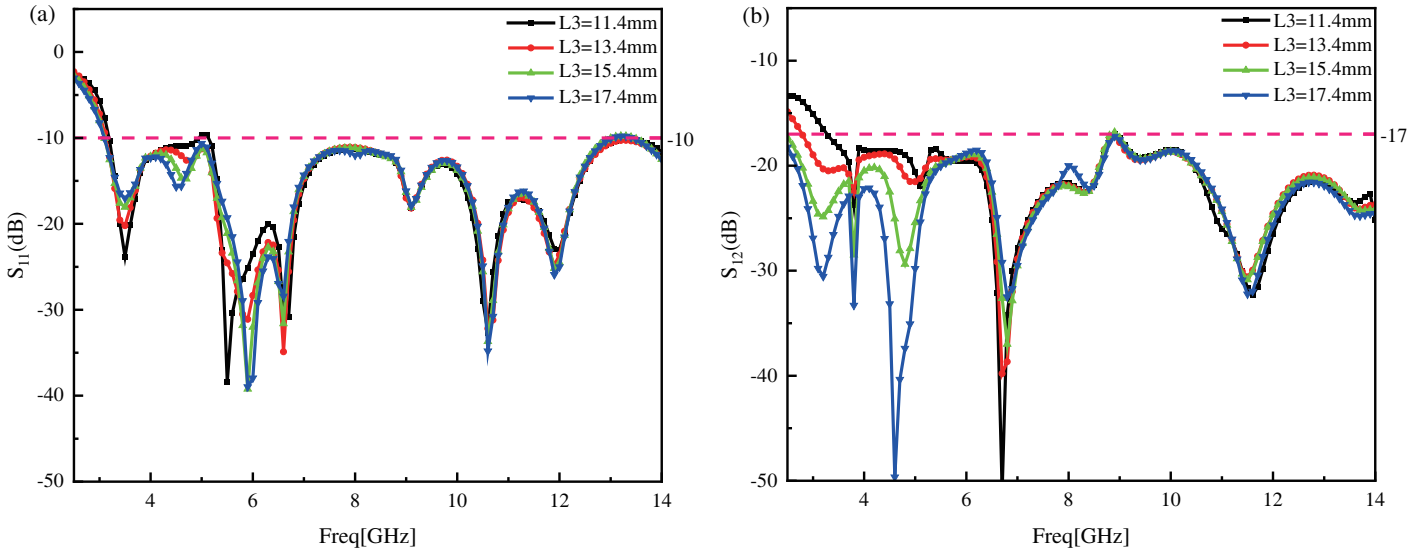

FIGURE 9. Effect of $L3$ parameter on antennas S_{11} and S_{12}: (a) S_{11}, (b) S_{12}.

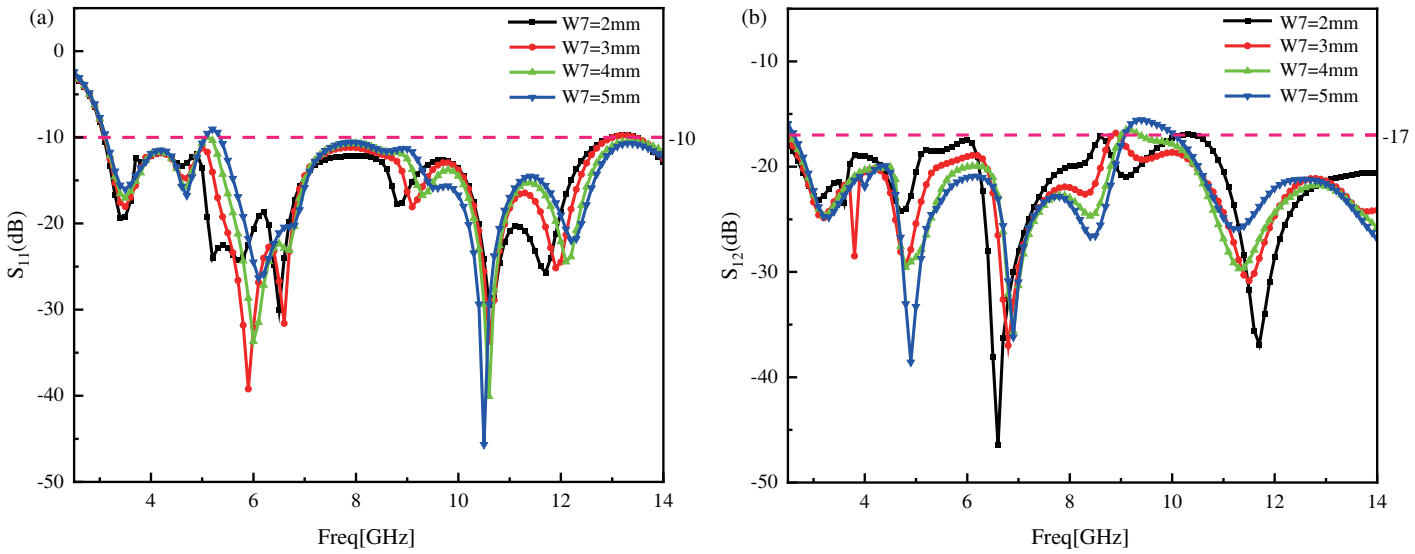

FIGURE 10. Effect of $W7$ parameter on antennas S_{11} and S_{12}: (a) S_{11}, (b) S_{12}.

added below it, with a large amount of current on the isolation structure, but a small amount of coupling current at port 2. In Figure 11(d), T-slots and inverted T-slots are used, the current at port 2 is minimized, and the isolation decoupling effect is optimized. Therefore, the antenna finally adopts the isolation decoupling structure of Figure 11(d), which blocks the current coupling between the ports and achieves the best isolation effect.

4. RESULTS AND DISCUSSION

4.1. S-Parameters

The frog-shaped UWB MIMO antenna proposed in this paper is simulated using HFSS software. To verify the actual performance of the antenna, the antenna model is physically processed, and the resulting prototype is shown in Figure 12. Antenna testing was conducted employing an Agilent N52235A vector network analyzer, with the test setup illustrated in Figure 13. The frequency range covered by the antenna, as shown in Figure 14, is 3.05–13.38 GHz, covering the n77, n78, n79, and 6 GHz bands for 5G as well as the UWB band from 3.1 to 10.6 GHz. In addition, the S_{12} parameter of the antenna stays below -17 dB in the operating bandwidth and below -20 dB in the n77, n78, n79, and 6 GHz bands, providing good isolation. Although there are some errors between the simulations and measurements of S_{11} and S_{12} shown in Figure 14, which may be caused by the fabrication process and test environment, they show a general similarity, with the overall performance of the antennas remaining consistent.

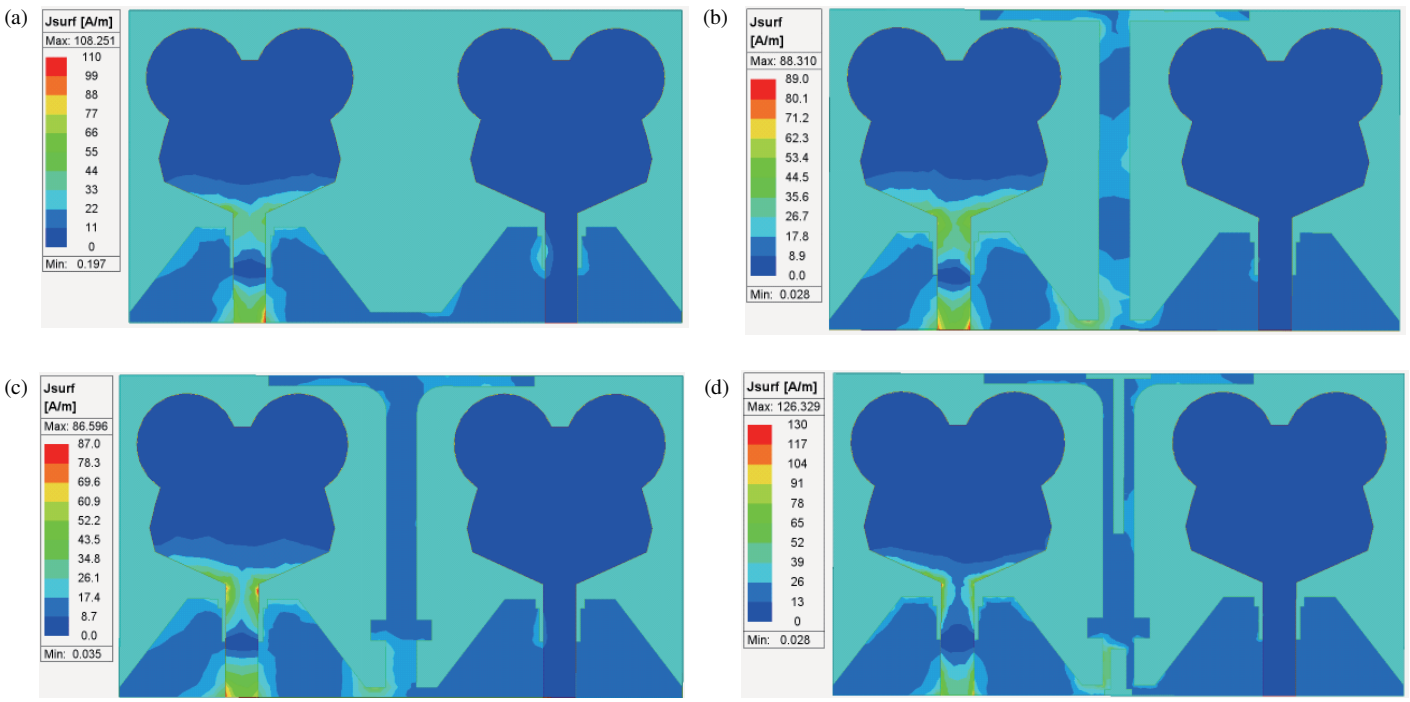

FIGURE 11. Surface currents of four floor-structured antennas: (a) Ant 1, (b) Ant 2, (c) Ant 3, (d) Ant 4.

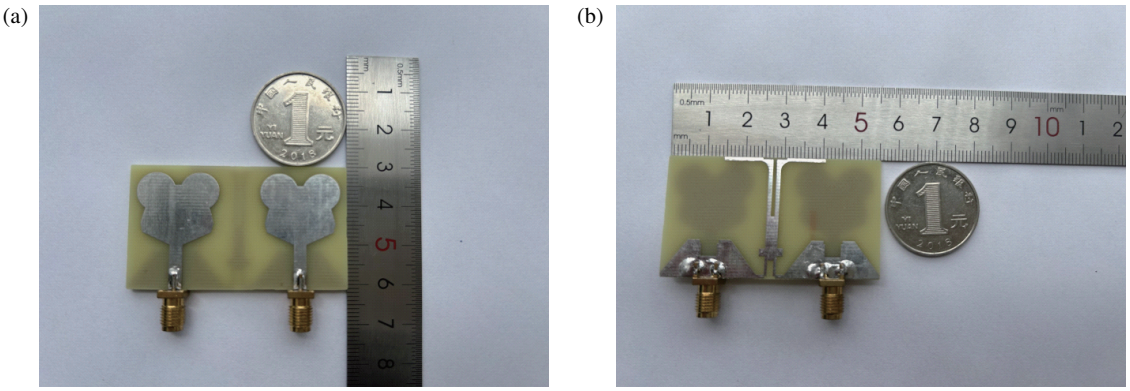

FIGURE 12. MIMO antenna fabrication prototype: (a) front of the antenna, (b) back of the antenna.

4.2. Radiation Properties

The radiation direction maps of the frog-shaped UWB MIMO antenna in the XOZ and YOZ directions were measured in a microwave anechoic chamber. Seven resonance points of the antenna were selected for the measurements. The results are shown in Figure 15. The observation can be made from Figure 15(a) that the antenna achieves omnidirectional radiation in the XOZ direction and maximum radiation gain directions of 0° and 180° in the YOZ direction at a frequency of 3.5 GHz. It can be seen from Figure 15(b) that the antenna achieves almost omnidirectional radiation in the XOZ and YOZ directions at a frequency of 4.7 GHz. It can be observed from Figure 15(c) that the antenna achieves omnidirectional radiation in the XOZ direction and maximum radiation gain in the YOZ direction in the directions of 30° and 150° at a frequency of 5.9 GHz. As can be seen from Figure 15(d), the maximum radiation direction of this antenna at 6.6 GHz is mainly distributed at 210°–330° for XOZ and 0°–60° and 120°–180° for YOZ. As can be seen in Figure 15(e), the maximum radiation directions of XOZ are mainly distributed in 0°–330° and 180°–230°, and the maximum radiation directions of YOZ are mainly distributed in 0°–30° and 140°–180° for this antenna at the frequency of 9.1 GHz. As can be seen from Figure 15(f), the maximum radiation directions of the antenna at 10.6 GHz are mainly distributed in 0°–340°, 240°–300° and 180°–220° for XOZ and 30°–320° and 220°–240° for YOZ. As can be seen in Figure 15(g), the antenna radiates nearly omnidirectionally in the XOZ plane at a frequency of 11.9 GHz, and the maximum radiation direction of the YOZ is mainly distributed in 180°–230°.

Figure 16 shows the maximum gain and radiation efficiency of the MIMO antenna. From Figure 16, the maximum value

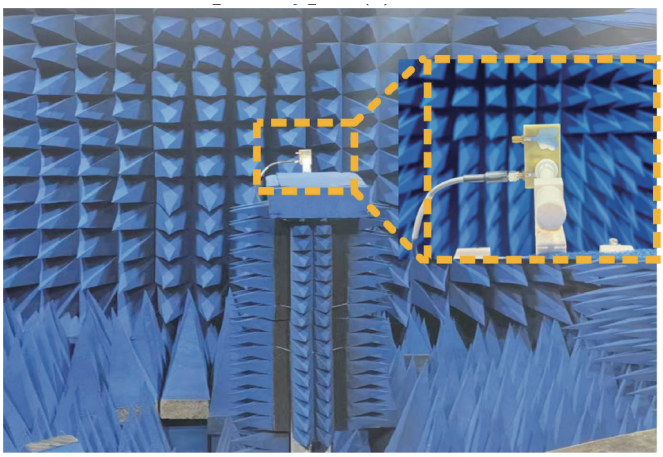

FIGURE 13. Antenna test environment.

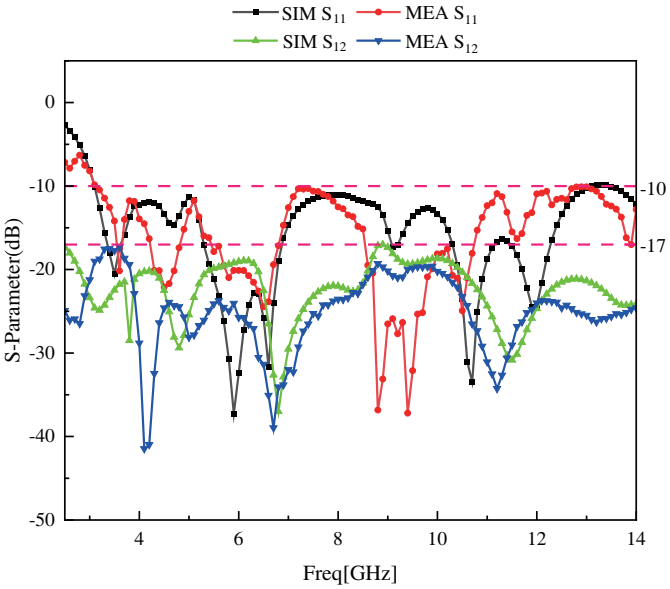

FIGURE 14. Simulated and measured S-parameters.

of the peak gain of the antenna (maximum gain of the radiating sphere) is 5.8 dBi. The radiation efficiency of the antenna ranges from 89% to 97%, and the antenna has excellent radiation performance as the radiation efficiency is consistently greater than 90% in the 3.05–13.38 GHz operating band. In consideration of the experimental conditions, the measured parameters for gain, radiation efficiency, co-polarization, and cross-polarization are not currently available.

4.3. MIMO Antenna Performance

4.3.1. ECC and DG

The correlation envelope coefficient (ECC) is the correlation of the received signal amplitude between different antenna units, which is used as a parameter index to evaluate the diversity performance and coupling performance of the MIMO multi-antenna system. The smaller the value of the ECC is, the smaller the inter-antenna unit influence is, and the better the MIMO antenna performance is. In general, for the antenna to work properly, the ECC value must be less than 0.5. ECC can be obtained from Equation (7) [19].

$$\mathrm{ECC} = \frac{\left|\iint_{4\pi}\left[\vec{F}_1(\theta,\varphi) * \vec{F}_2(\theta,\varphi)\right] d\Omega\right|^2}{\iint_{4\pi}\left|\vec{F}_1(\theta,\varphi)\right|^2 d\Omega \iint_{4\pi}\left|\vec{F}_2(\theta,\varphi)\right|^2 d\Omega} \tag{7}$$

As shown in Figure 17, the maximum value of ECC of this antenna is about 0.007 in the operating band and less than 0.005 in most of the frequencies.

Diversity gain (DG) is another performance metric of the MIMO antenna that can be calculated from the ECC, and the closer its value is to 10 dB, the better the antenna works. Equation (8) is calculated as follows:

$$\mathrm{DG} = 10 \times \sqrt{1 - \mathrm{ECC}} \tag{8}$$

As shown in Figure 18, the antenna has a minimum value of DG in the operating band of 9.96 dB. Therefore, the antenna has good diversity performance.

4.3.2. TARC and CCL

Total active reflection coefficient (TARC) is an important performance metric for MIMO antennas. It indicates the effective bandwidth of a MIMO antenna when multiple ports are excited simultaneously and can be calculated using the S-parameter. In general, a TARC value less than -10 dB in the frequency band is considered to design an antenna with low reflection loss and good phase stability. Equation (9) for calculating the TARC of a two-port MIMO antenna is given below:

$$\mathrm{TARC} = \sqrt{\frac{(S_{11}+S_{12})^2 + (S_{21}+S_{22})^2}{2}} \tag{9}$$

Figure 19 shows the TARC of the antenna, which is below -30 dB in the operating band, indicating good antenna decoupling.

Channel capacity loss (CCL) is also an important parameter in MIMO antennas to measure the channel capacity loss between the antenna transceivers. Generally, the channel capacity loss of the antenna is considered acceptable if the CCL is less than 0.4 bit/s/Hz. CCL can be calculated by Equations (10), (11), (12), and (13).

$$\mathrm{CCL} = -\log_2 \det\left(\alpha^R\right) \tag{10}$$

$$\alpha^R = \begin{bmatrix} \alpha_{11} & \alpha_{12} \\ \alpha_{21} & \alpha_{22} \end{bmatrix} \tag{11}$$

$$\alpha_{ii} = 1 - \left|\sum_{n=1}^{2} S_{in} * S_{ni}\right| \tag{12}$$

$$\alpha_{ij} = -\left|\sum_{n=1}^{2} S_{in} * S_{nj}\right| \tag{13}$$

Figure 20 illustrates the CCL of the antenna, which is less than 0.34 bit/s/Hz across the operating band, indicating the high reliability of the antenna.

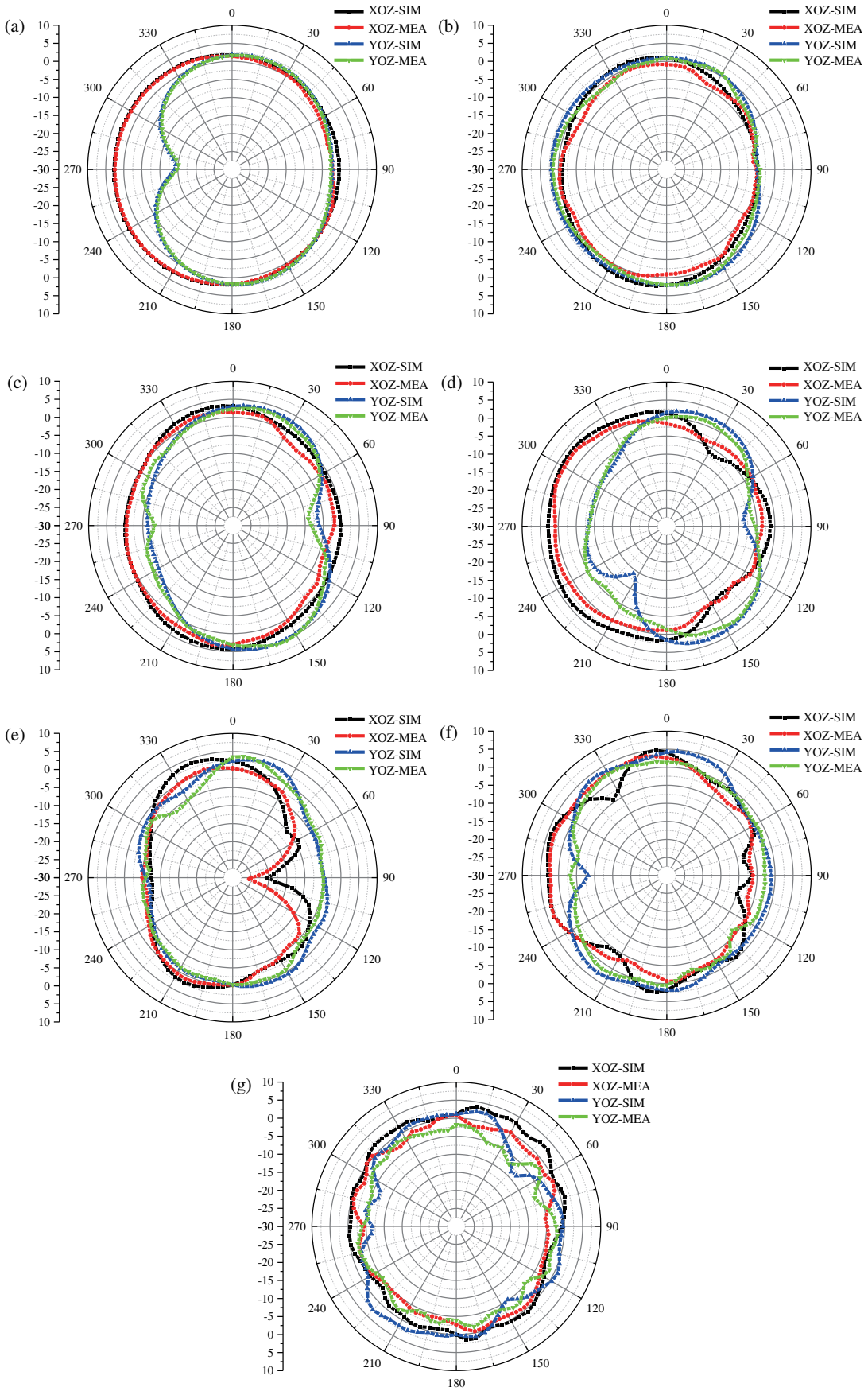

FIGURE 15. Simulated and measured orientation diagrams: (a) 3.5 GHz, (b) 4.7 GHz, (c) 5.9 GHz, (d) 6.6 GHz, (e) 9.1 GHz, (f) 10.6 GHz, (g) 11.9 GHz.

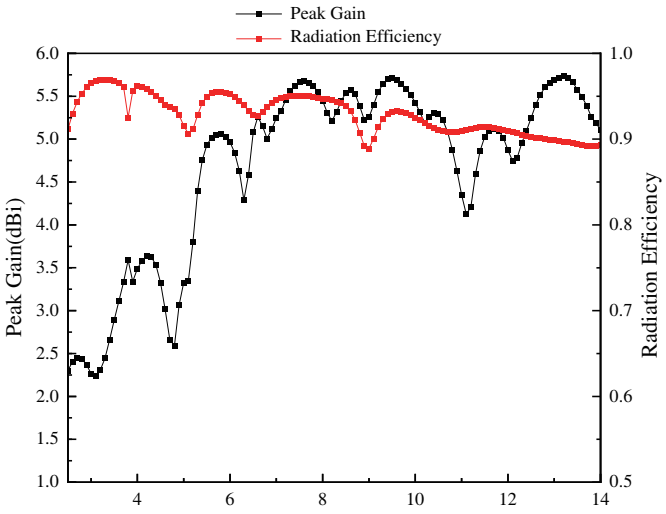

FIGURE 16. Peak gain and radiation efficiency of the antenna.

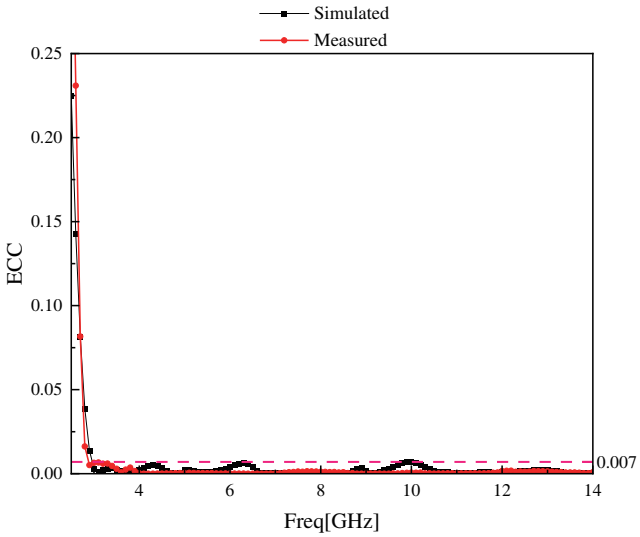

FIGURE 17. Simulating and measuring ECC.

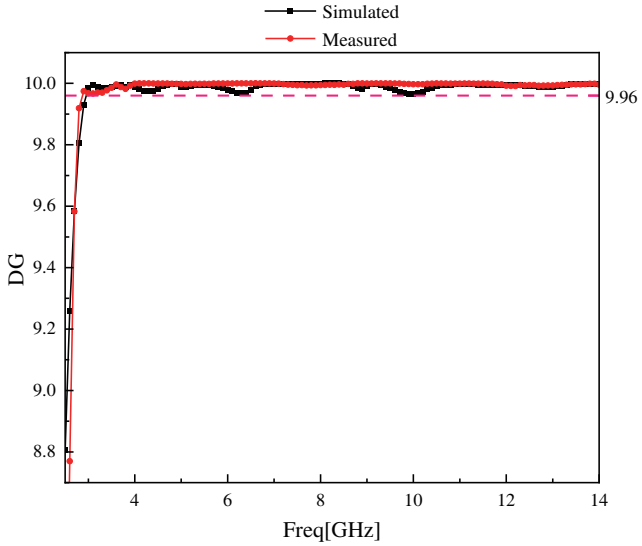

FIGURE 18. Simulating and measuring DG.

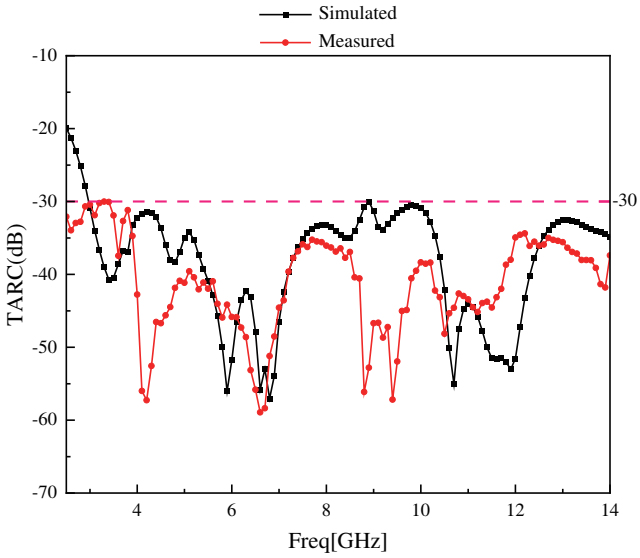

FIGURE 19. Simulating and measuring TARC.

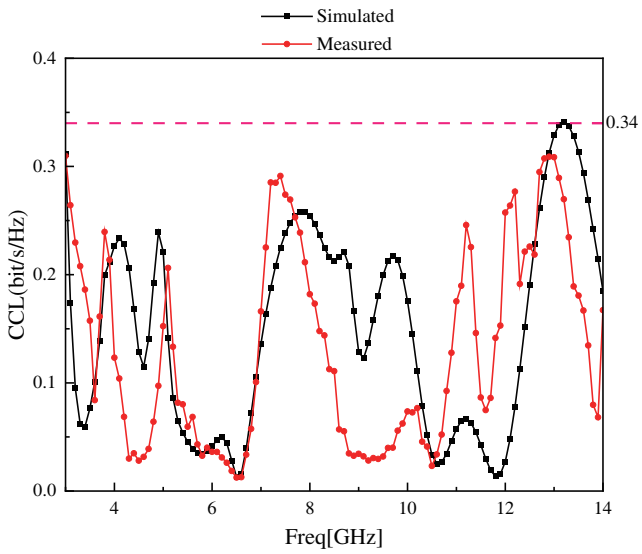

FIGURE 20. Simulating and measuring CCL.

TABLE 3. Comparison of the proposed antenna with several existing antennas.

Ref	Size (λ_0^2)	Bandwidth (GHz)	Isolation (dB)	ECC	Radiation Efficiency (%)
[7]	0.23×0.32	2–18	< -15	< 0.07	70–90
[12]	0.95×1.50	3.55–3.8 4.6–4.8	< -14	< 0.04	90–97
[15]	0.83×0.83	2.77–12	< -15	< 0.1	75–82
[16]	0.71×0.73	3.5–11	< -20	< 0.01	70–90
[20]	0.26×0.51	2.4–10.2	< -17	< 0.15	60–85
[21]	0.20×0.40	2.3–11.5	< -16	< 0.012	82–96
[22]	0.31×0.43	2.56–12	< -20	< 0.01	-
This Work	$\mathbf{0.32 \times 0.56}$	**3.05–13.38**	$\mathbf{< -17}$	$\mathbf{< 0.007}$	**89–97**

5. COMPARE WITH EXISTING ANTENNAS

Table 3 shows the comparison of the antenna proposed in this paper with several existing antennas in terms of size, bandwidth, isolation, ECC, and radiation efficiency. The proposed antenna has smaller dimensions than [12, 15, 16]. The bandwidth of the antenna is wider than [12, 15, 16, 20–22]. The antenna provides better isolation than [7, 12, 15, 21] and lower ECC than [7, 12, 15, 16, 20–22]. The radiation efficiency is higher than those of [7, 15, 16, 20, 21], which are basically above 90%. Therefore, the antenna proposed in this paper has better performance.

6. CONCLUSION

In this paper, a compact frog-shaped UWB MIMO antenna is designed for 5G applications in n77, n78, n79, and 6 GHz bands. The antenna consists of two frog-shaped metal patches with an improved T-shaped defective floor structure with T-slots on the T-shaped floor to realize decoupling between the antenna ports. The isolation effect of the antenna is always below -17 dB. The antenna operates in the range of 3.05–13.38 GHz, covering UWB (3.1–10.6 GHz). The antenna has seven resonances: 3.5 GHz, 4.7 GHz, 5.9 GHz, 6.6 GHz, 9.1 GHz, 10.6 GHz, and 11.9 GHz. Three of these resonances, 3.5 GHz, 4.7 GHz, and 6.6 GHz, are in the range of n77 (3.3–4.2 GHz), n78 (3.3–3.8 GHz), n79 (4.4–5 GHz), and 6 GHz band (6.4–7.1 GHz). In the MIMO antenna diversity performance metrics, the ECC is less than 0.007, the DG more than 9.96, the TARC less than -30 dB, and the CCL less than 0.34 bit/s/Hz. As a result, the proposed UWB MIMO antenna is suitable for low and medium frequency 5G wireless applications.

ACKNOWLEDGEMENT

This work was partially supported by the National Natural Science Foundation of China (No. 62105004) and the Natural Science Research Program for Universities in Anhui Province (No. KJ2020A0308).

REFERENCES

[1] Ministry of Industry and Information Technology, "Regulations of the people's republic of China on the division of radio frequencies," 1–241, China, 2023.

[2] Federal Communications Commission 47 CFR Part 15, Vol. 67, "Ultra-wideband transmission systems," 34 852–34 860, 2002.

[3] Molisch, A. F. and M. Z. Win, "MIMO systems with antenna selection," *IEEE Microwave Magazine*, Vol. 5, No. 1, 46–56, 2004.

[4] Paulraj, A. J., D. A. Gore, R. U. Nabar, and H. Bolcskei, "An overview of MIMO communications — A key to gigabit wireless," *Proceedings of the IEEE*, Vol. 92, No. 2, 198–218, 2004.

[5] Daghari, M., C. Essid, and H. Sakli, "Muli-UWB antenna system design for 5G wireless applications with diversity," *Wireless Communications and Mobile Computing*, Vol. 2021, No. 1, 9966581, 2021.

[6] Addepalli, T. and V. R. Anitha, "Parametric analysis of compact UWB-MIMO antenna with improved isolation using parasitic reflectors and protruded ground strips," *Wireless Personal Communications*, Vol. 123, No. 3, 2209–2225, 2022.

[7] Sakli, H., C. Abdelhamid, C. Essid, and N. Sakli, "Metamaterial-based antenna performance enhancement for MIMO system applications," *IEEE Access*, Vol. 9, 38 546–38 556, 2021.

[8] Ahmed, B. T., "High isolation compact UWB MIMO antennas," *Wireless Personal Communications*, Vol. 128, No. 4, 3003–3029, 2023.

[9] Siyara, J. P., M. N. Jiyani, O. Alsalman, S. P. Lavadiya, and S. K. Patel, "Novel metamaterial array-based dual port MIMO antenna using low profile substrate with feature multiband, and high isolation for sub-6G, IoT, and WiMAX applications," *Physica Scripta*, Vol. 99, No. 9, 095531, 2024.

[10] Zeain, M. Y., M. Abu, A. A. Althuwayb, H. Alsariera, A. J. A. Al-Gburi, A. A. Abdulbari, and Z. Zakaria, "A new technique of FSS-based novel chair-shaped compact MIMO antenna to enhance the gain for sub-6 GHz 5G applications," *IEEE Access*, Vol. 12, 49 489–49 507, 2024.

[11] Kumar, P., R. Sinha, A. Choubey, and S. K. Mahto, "DGS based miniaturized wideband MIMO antenna with efficient isolation for C band applications," *Frequenz*, Vol. 77, No. 3-4, 163–172, 2023.

[12] Chakraborty, S., M. A. Rahman, M. A. Hossain, E. Nishiyama, and I. Toyoda, "A novel dual-band elliptical ring slot MIMO antenna with orthogonal circular polarization for 5G applications,"

Heliyon, Vol. 10, No. 13, e33176, 2024.

[13] Li, W., L. Wu, S. Li, X. Cao, and B. Yang, "Bandwidth enhancement and isolation improvement in compact UWB-MIMO antenna assisted by characteristic mode analysis," *IEEE Access*, Vol. 12, 17 152–17 163, 2024.

[14] Shariff, B. G. P., T. Ali, P. R. Mane, P. Kumar, and S. Pathan, "Compact wideband two-element millimeter wave MIMO antenna with CMT based modified T-shaped decoupling structure for mobile applications with estimated link budget in urban scenario," *AEU — International Journal of Electronics and Communications*, Vol. 177, 155209, 2024.

[15] Alharbi, A. G., U. Rafique, S. Ullah, S. Khan, S. M. Abbas, E. M. Ali, M. Alibakhshikenari, and M. Dalarsson, "Novel MIMO antenna system for ultra wideband applications," *Applied Sciences*, Vol. 12, No. 7, 3684, Apr. 2022.

[16] Abdelghany, M. A., M. F. A. Sree, A. Desai, and A. A. Ibrahim, "4-Port octagonal shaped MIMO antenna with low mutual coupling for UWB applications," *Computer Modeling in Engineering & Sciences*, Vol. 136, No. 2, 1999–2015, 2023.

[17] Saleem, S., S. Kumari, D. Yadav, M. G. Siddiqui, and D. Bhatnagar, "A planar UWB-MIMO antenna with high isolation and reconfigurable single band-elimination characteristics," *AEU — International Journal of Electronics and Communications*, Vol. 170, 154853, 2023.

[18] Kansal, P., A. K. Mandpura, and N. Kumar, "Triple band self-decoupled MIMO antenna pair for 5G communication," *Physica Scripta*, Vol. 99, No. 9, 095532, 2024.

[19] Sharawi, M. S., "Printed multi-band MIMO antenna systems and their performance metrics [wireless corner]," *IEEE Antennas and Propagation Magazine*, Vol. 55, No. 5, 218–232, 2013.

[20] Mohanty, A. and B. R. Behera, "Insights on radiation modes and pattern diversity of two element UWB fractal MIMO antenna using theory of characteristics modes analysis," *AEU — International Journal of Electronics and Communications*, Vol. 135, 153726, Jun. 2021.

[21] Kiani, S. H., H. S. Savci, M. E. Munir, A. Sedik, and H. Mostafa, "An ultra-wide band MIMO antenna system with enhanced isolation for microwave imaging applications," *Micromachines*, Vol. 14, No. 9, 1732, 2023.

[22] Du, C. and H. Peng, "Cpw-fed UWB-MIMO antenna with triple-band notched and high isolation using double Y-shaped decoupling structure," *The Applied Computational Electromagnetics Society Journal (ACES)*, 903–913, 2023.